Virtual Super Resolution of Scale Invariant Textured Images Using Multifractal Stochastic Processes

Pierre Chainais, Emilie Koenig, Véronique Delouille, Jean-François Hochedez

Journal of Mathematical Imaging and Vision manuscript No.
(will be inserted by the editor)

Virtual super resolution of scale invariant textured images using multifractal stochastic processes

Pierre Chainais · Émilie Kœnig · Véronique Delouille · Jean-François Hochedez

Received: date / Accepted: date

Abstract We present a new method of magnification for textured images featuring scale invariance properties. This work is originally motivated by an application to astronomical images. One goal is to propose a method to quantitatively predict statistical and visual properties of images taken by a forthcoming higher resolution telescope from older images at lower resolution. This is done by performing a virtual super resolution using a family of scale invariant stochastic processes, namely compound Poisson cascades, and fractional integration. The procedure preserves the visual aspect as well as the statistical properties of the initial image. An augmentation of information is performed by locally adding random small scale details below the initial pixel size. This extrapolation procedure yields a potentially infinite number of magnified versions of an image. It allows for large magnification factors (virtually infinite) and is physically conservative: zooming out to the initial resolution yields the initial image back. The (virtually) super resolved images can be used to predict the quality of future observations as well as to develop and test compression or denoising techniques.

Keywords natural images · scale invariance · multifractal analysis · extrapolation · enhancement · infinitely divisible cascades

P. Chainais, É. Kœnig
Clermont Université, Université Blaise Pascal
CNRS UMR 6158, LIMOS
BP10448, F-63000 Clermont-Ferrand, France
E-mail: pchainai@isima.fr, koenig@isima.fr

V. Delouille, J.-F. Hochedez
Royal Observatory of Belgium
Avenue Circulaire 3, B-1180 Brussels
E-mail: v.delouille@sidc.be, hochedez@sidc.be

1 Introduction

We present a new method to magnify random textured images by any factor (even much larger than 2) while preserving their visual aspect as well as their statistical properties. Such a method will add small scale details below the initial pixel size by proposing some plausible guess of what might be hidden under the available resolution, see figure 1. As a consequence, an augmentation of information is performed. This work was originally motivated by various applications to remote sensing for geophysics and astrophysics as well as to computer graphics. The purpose of our approach is to propose a reasonable set of predictions of what the small scales might be. In astrophysics, no instrument will likely ever resolve all relevant physical scales. One would like to be able to simulate realistic high resolution images extrapolated from currently badly resolved ones. Compression algorithms or denoising techniques could then be optimized and validated using these virtually super-resolved images as a reference. For instance, in solar physics, current observations from the Extreme ultraviolet Imaging Telescope onboard SOHO are 1024×1024 images at resolution 1800km [18]. Therefore, physicists are considering the design of a new spatial telescope with a much better resolution of 80km which is about 25 times finer than that of EIT. Virtually super-resolved images may help to design and calibrate various image processing procedures before there embedding. Moreover, as the resolution gets finer, the flux of photons on the CCD sensor gets smaller so that the images may be under-exposed and unusable. Since the present approach preserves statistical properties, statistical quantities such as histograms of intensity at finer resolutions can be predicted in good approximation provided the assumption of scale invariance remains valid over the range of scales that is considered. The expected quality of future images can then be reasonably estimated. Such an approach may be useful in

other remote sensing contexts where turbulent physical systems like galaxies or clouds are observed. Virtual super-resolution of textures may be useful in computer graphics as well. The purpose is then to compute small scale details if they are visible only. Indeed textures play a crucial role in the æsthetic rendering but also use a lot of memory space when stored at full resolution. Procedural texture synthesis [19] permits to synthesize textures (ideally on the fly) at sufficient resolution for rendering. For instance, when a character moves towards some object in a scene, it is desirable to be able to synthesize new details gradually thanks to an online enhancement of the texture. The visual aspect of some random texture is a direct consequence of the statistical properties of the underlying stochastic process. Therefore we are faced with the same kind of problem as evoked above for astronomy. Virtual super-resolution will then aim at the rendering of better resolved textures by generating new details at arbitrary resolution. More generally this approach may be used to enhance textured regions in a segmented image.

Our approach relies on the fact that natural images as well as many random textures usually present scale invariance properties [19, 49]. More precisely, the present work deals with scale invariant textured images in particular, such as obtained by the remote sensing of turbulent systems like the Sun, clouds or stellar systems for instance. The main thrust is to consider images as realizations of some stochastic process and to propose a reasonable extrapolation of their scale invariance properties at arbitrarily small scales, below the initial pixel size. We perform some kind of stochastic interpolation in the *spatial* domain by extrapolating multifractal properties in the *scale* domain. Therefore, we speak of virtual super resolution since we do not aim at a deterministic prediction of some under-resolved existing information but rather at proposing a set of realizations of some plausible underlying information. To this purpose, we require that the content of the augmented image be *consistent* with the information available at larger scales from the original image. We define this consistency by two requirements: the preservation of scale invariance properties of the initial image *(statistical consistency)* and the conservation of the energy flux, that is zooming out to the initial resolution must yield the original image back *(physical consistency)*. As a consequence, this approach uses minimal assumptions and introduces some prior through fundamental properties only.

Several approaches to enlargement by interpolation or super-resolution have already been proposed in the literature. The enlargement of images implies the apparition of new pixels. This calls for some assumptions on the image itself to design some interpolation method. Beyond Shannon interpolation, B-spline based techniques have been proposed to enlarge or reduce regular images [53] and to overcome the limitation of the usual band-limited assumption [54]. Generalized interpolation techniques [33, 51] have also been proposed to reach a better quality of approximation than traditional interpolation.

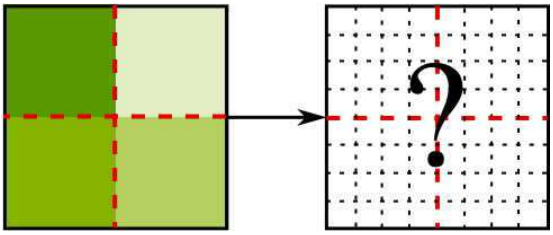

Fig. 1 Position of the problem : how to propose some plausible guess of what might be hidden under the available resolution ? New sub-pixel details will be introduced, under some physical and statistical constraints.

Some approaches have proposed to take into account the importance of edges in natural images. The basic idea in [39] was to estimate local covariance coefficients of a low-resolution image to adapt the high-resolution covariance. Despite its large computational complexity, this method gives very nice results for cartoon-like images. In [20], a statistical modeling of edges and a maximum likelihood estimate are used to propose an edge preserving upsampling. While they interestingly preserve local anisotropy, such approaches are not suited to texture images where edges are not expected to be the key features.

In a slightly different spirit, some works propose to preserve the local Hölderian regularity of the image which is equivalent to preserve some locally scale invariant behavior. One possibility is to learn some codebook mapping between low-resolution and high-resolution patches [50]. Other authors use the scaling behaviour of wavelet coefficients around a singularity to extrapolate a new wavelet subband at higher resolution [8, 16, 37]. One limitation may be that once the wavelet is chosen, this extrapolation is deterministic and the result may be noticeably affected by the chosen wavelet. Moreover, the main purpose is in general more to sharpen the edges rather than to preserve scale invariant textures.

Aiming at a better processing of textured regions, several approaches have proposed to use some prior knowledge of higher resolution information. This is the basic idea of example based super-resolution [22] where the system first learns a set of correspondences between low-resolution and high-resolution patches. The same kind of idea has been developed in more recent works. In [38], a data-driven parametric model in the wavelet domain is used. In [27], texture hallucination is introduced, that is high-resolution patches are chosen in a dataset of examples. These approaches assume the knowledge of high resolution information which is not available in our case.

A very interesting approach has been proposed in [24] to overcome this drawback by exploiting the scale invari-

ance of the image itself, in the spirit of NL-means methods. The main idea is to take benefit from patch redundancy in a single image: the low-res/high-res patch correspondences are learnt directly from the image and its coarsened versions at various scales. This approach implicitly uses the internal self-similarity of a single image to extrapolate information at high resolution. The visual result is very nice and accurate both for edges and textures. However, we have no guarantee that quantitative statistical properties will be correctly extrapolated, in particular when applying an enlargement by a factor much larger than 2 like 16 or 32 for instance.

Note that the various approaches above were designed to process either cartoon-like images (smooth regions separated by edges) or more textured images with prior knowledge of textures at small scales. The former do not aim at adding much information at sub-pixel scales, but rather at being as faithful as possible to the fully resolved reality underlying some sufficiently regular image. In the latter, small scale information is supposed to be available within some data base of patches for instance. When dealing with remote sensing images of disordered (turbulent) scenes, we fall out of the assumptions of all these methods since there are no clearly visible edges and we do not know what small scales consist of because of observational limitations. As a consequence, we will work in two steps: first enlarge the image thanks to any regularity preserving technique, and then add new details considering the image as a stationary scale invariant random field; we are not much concerned about edges here.

As far as the interpolation of stationary random fields is concerned, some authors [26, 28] have explored the potential of fractal interpolation by modeling the image as a fractional Brownian motion (fBm). Due to the local roughness of the fBm, one expects that the visual aspect of textured regions be better preserved than with usual interpolation methods which enforce some kind of regularity of the resulting image. More recently, wavelet fractal interpolation was proposed to enlarge remote sensing satellite images of the Earth [26]. The idea is to apply a fractal interpolation in the wavelet domain. In these approaches, the model is Gaussian and works with second order correlations only.

Still in the stream of fractal interpolation, Iterated Function Systems (IFS) [2] have also been proposed with some success for compression and interpolation. An IFS can be used to model an image as the fixed point of some iterated function transformation. Interpolation using IFS consists in applying another iteration of the initial IFS determined thanks to the collage theorem. Such an approach preserves scale invariance in a very elegant framework. However it remains deterministic and does not ensure the controlled extrapolation of the higher order multifractal behavior of the initial image since the IFS remains an implicit model. Another possibility relies on the use of Hidden Markov Random Fields. The idea is to propose an enhanced version of some low resolution image by using a hierarchical hidden field [40]. By constructing hierarchical hidden fields, which label the behaviour type, such an approach may be able to capture heterogeneous structure in a scale-dependent way. This method has been applied to the resolution enhancement of porous media binary images. Among other limitations, this method calls for the learning of statistical quantities from high resolution images so that the knowledge of the small-scale structure is needed. An exact prediction is then expected. Last, this approach has been proposed for binary images only and an important limitation is that fractal-like images are difficult to deal with by using such methods until now.

The originality of our approach lies in several main ingredients. We consider the image intensity as a measurement of the energy carried by the photon flux. Therefore, our technique will assume an energy conservation rule: the super resolved image must give the initial image back when degrading the image back to the initial resolution. Another originality of our approach lies in its stochastic nature: we do not aim at proposing a unique version of the virtual high resolution image but rather at proposing a plausible set of realizations that may be underlying some given low resolution image. By plausible, we mean that the high resolution image must obey the same scale invariance properties as the original image but over a wider range of scales. We will always implicitly assume that original images are very much under resolved and that scale invariance holds over a wide range of scales below the initial pixel size. Last, let us emphasize that we speak of *virtual* super resolution here, since small scales are introduced by a model. This model relies on a family of multifractal stochastic processes, namely compound Poisson cascades (CPC) [4, 12, 13, 42], combined to fractional integration understood as a scale invariant low pass filtering in the Fourier domain. The core of our approach lies in the multiscale multiplicative structure of CPC: the high-resolution version of a CPC can be decomposed as the product of a low-resolution CPC and an independent intermediate CPC carrying small scale information, see eq. (14). Parts of the results presented in this article were communicated to ICIP'09 [34] and to GRETSI'09 [35].

The article is organized as follows. Section 2 recalls on some definitions and properties of compound Poisson cascades and multifractal processes. We also briefly review the interest of such stochastic processes for the modeling of natural images and textures. Section 3 presents our approach in details and explains the virtual super resolution procedure. Section 4 studies the behavior of this approach thanks to some numerical experiments and analyses. We also show how such an approach can be useful for an application to astronomical images of the Sun. Section 5 summarizes our main results and points to directions for future work.

2 Multifractal processes to model the statistics of natural images

2.1 Scale invariance of natural images

The statistics of natural images have been studied in depth [49]. They have revealed two main properties: scale invariance and non-Gaussian statistics. This is also true for a large variety of "random textures" [19] so that many models for natural images can be used to synthesize random textures as well. The scale invariance of natural images is basically characterized by the power law Fourier spectrum of the image intensity $\propto 1/k^{2-\eta}$ over a wide range of spatial frequencies. It is noticeable that this behavior is very often observed in good approximation even for one single natural image. In the spatial domain, this behavior is equivalent to power law correlations at least for some range of small scales. This scale invariance can be characterized in an even more precise framework for higher order statistics as well [12, 52]. Let $T_I(r)$ be a multiscale transform (wavelets, box averages...) at scale r of the image I under study. The scale invariance property results in the power law scaling behavior $\mathbb{E}T_I(r)^q \propto r^{\zeta(q)}$, $q \in \mathbb{R}$ where $\mathbb{E}$ stands for mathematical expectation. The $\zeta(q)$ are called *multifractal* or *multiscaling exponents*. They capture higher order dependences. They can be decomposed in a linear part qH depending on a parameter H and a non-linear part $\tau(q)$, such that $\tau(0) = \tau(1) = 0$ and $H = \zeta(1)$. Then $\zeta(q) = qH + \tau(q)$. For instance in the case $\zeta(q) = qH$ (e.g. a fractional Brownian field), the image I is said self-similar and its scale invariance is characterized by the parameter H only. When the non linear part $\{\tau(q), q \in \mathbb{R}\}$ exists and is not identically zero, a set of exponents is necessary to describe the scale-invariance of the image. The nonlinearity of $\tau(q)$ betrays a multiscaling property which also depicts the non-Gaussianity of the image statistics. For a multiscaling image, the parameters H and $\tau(q)$ are linked to the power law Fourier spectrum which is $\propto 1/k^{2+2H+\tau(2)}$ [12]. Next section is a brief presentation of the notion of statistical scale invariance of stochastic processes.

2.2 Statistical scale invariance

As we will make use of scale invariant stochastic processes, we give a short presentation of the notion of scale invariance for stochastic processes. To this aim, let us first recall the link between scale invariance and power laws. In the deterministic framework, an object is said to be self-similar when it remains invariant through dilations. One simple example is the set of functions on $\mathbb{R}^+$ such that, for some $H \in \mathbb{R}$,

$$\forall c \in \mathbb{R}^+, \quad f(ct) = c^H f(t). \tag{1}$$

It is well known that this is the set of power laws $f(t) = a\,t^H$ where a is a constant, $H \in \mathbb{R}$. In the stochastic framework, one speaks of statistical self-similarity when the correspondence between descriptions of the same object at different scales are expressed in terms of equalities in laws denoted by $\stackrel{d}{=}$ below. A stochastic process $X(t)$ indexed by $t \in \mathbb{R}$ with values in $\mathbb{R}$ is self-similar with Hurst parameter H if:

$$\forall c \in \mathbb{R}^+, \quad \{X(ct), t \in \mathbb{R}^+\} \stackrel{d}{=} c^H \{X(t), t \in \mathbb{R}^+\}. \tag{2}$$

The archetype of self-similar processes is the fractional Brownian motion (fBm) denoted by $B_H(t)$. Note that the fBm is the only Gaussian process which is self-similar with stationary increments. In 2 dimensions, the notion of self-similarity can be generalized to other operators than natural dilation by possibly introducing some anisotropy [7]. A more flexible framework corresponds to the multiscaling scale invariance property:

$$\forall c \in [0,1], \{X(ct), t \in [0,T]\} \stackrel{d}{=} W_c \cdot \{X(t), t \in [0,T]\} \tag{3}$$

where T is a large scale beyond which the property cannot be true anymore; W_c is a random variable independent of X. In this work, we will consider the particular case where $W_c = c^H e^{\Omega_c}$ where Ω_c is a random variable such that $\mathbb{E}e^{q\Omega_c} = c^{\tau(q)}$ for relevant values of q ($\tau(q)$ is a concave function). Then $\mathbb{E}W_c^q = c^{qH+\tau(q)}$. We speak of multiscaling processes. In practice only processes with stationary increments are easy to use for modelling purpose. Therefore, we will consider scale invariant processes with stationary increments only. In this case, the moments of the absolute value of the increments $\delta_r X(t) = X(t+r) - X(t)$ behave as (if they are well defined)

$$\mathbb{E}|\delta_r X|^q = \mathbb{E}|\delta_1 X|^q \, r^{\zeta(q)} \tag{4}$$

where $\zeta(q) = qH + \tau(q)$ and $r \in [0,\ T]$. Such processes are also called *multifractal*. Their scale invariance properties are described by the set of multifractal exponents $\zeta(q)$. These exponents carry information on higher order correlations. Very often, eq. (4) also holds for wavelet coefficients. This is important as far as data analysis is concerned because when wavelet based estimates of exponents $\zeta(q)$ are relevant, they are also more accurate and efficient than those based on increments [17, 30, 32, 36, 43, 46, 57]. This is worth being mentioned since the virtual super resolution method described in this work calls for a preliminary multifractal analysis of the original image, that is the estimation of the exponents $\zeta(q)$. Finally, note that self-similarity is recovered when $\forall q, \tau(q) = 0 \Leftrightarrow \Omega_c = 0$ and the process is then said monofractal with $\zeta(q) = qH$.

To the purpose of modelling data from turbulent flows in fluid mechanics, some authors have empirically proposed an even more general framework, namely infinitely divisible multiscaling [9–11]. This general framework later raised the

basic ideas to build multifractal measures and processes. Infinitely divisible multiscaling is defined by the general scaling property (for instance for absolute values of wavelet coefficients)

$$\mathbb{E}T_X(r)^q = c_q \exp[-H(q)\cdot n(r)] \tag{5}$$

where $n(r)$ can be some non increasing function of r and $e^{-H(q)} = \mathbb{E}e^{q\omega}$ is the moment generating function of an infinitely divisible random variable ω [21]. The classical power laws of multifractal scaling are recovered when

$$\begin{cases} n(r) &= -\log r, \\ \mathbb{E}T_X(r)^q &= c_q r^{H(q)}. \end{cases} \tag{6}$$

Then $H(q)$ can be identified to multifractal exponents $\zeta(q)$. However, more general scale dependences can be considered and are sometimes called extended self-similarity [6, 52]. This approach is important since it opened the way to the construction of infinitely divisible cascades [48]. Indeed it makes a bridge between multiscaling properties and the intuition that multiplicative cascades may be of some help to define multiscaling stochastic processes (see eq. (9) below). In this approach a scale evolution equation can be written for $\mathbb{E}T_X(r)^q$:

$$\mathbb{E}T_X(r_2)^q = \mathbf{e}^{-H(q)[n(r_2)-n(r_1)]}\cdot \mathbb{E}T_X(r_1)^q \tag{7}$$

for scales $r_2 \leq r_1$. Let us recall that the product of moment generating functions is associated to the convolution of corresponding distributions, which is itself associated to the sum of independent random variables. Assume that $\tilde{G}(q) = e^{-H(q)}$ is the moment generating function of an infinitely divisible random variable $\omega = \log W$ [21]. Denote $Y = \log T_X$ so that $\mathbb{E}T_X^q = \mathbb{E}e^{qY}$. Then eq.(7) can be rewritten as

$$P_{r_2}(Y) = G^{*[n(r_2)-n(r_1)]} * P_{r_1}(Y), \tag{8}$$

where $P_r(Y)$ is the distribution of $Y = \log T_X$ at scale r and $G^{*[n(r_2)-n(r_1)]}$ must be read as an iterated convolution corresponding to $\tilde{G}(q)^{[n(r_2)-n(r_1)]}$, the moment generating function of a random variable $\omega_{r_1,r_2} = \log W_{r_1,r_2}$. Below we will denote $W_{r_1,r_2} = W^{[n(r_2)-n(r_1)]}$ with little abuse. This equation shows that the evolution of the distribution of $T_X(r)$ with scale r is controlled by the so-called propagator G and the scale dependence $n(r)$. Another consequence of eq.(8) is that one may translate eq.(7) as a multiplicative underlying structure described by the equality in law (with little abuse of notation):

$$T_X(r_2) \stackrel{d}{=} W^{[n(r_2)-n(r_1)]}\cdot T_X(r_1). \tag{9}$$

This short presentation points to the deep link between multiscaling processes and multiplicative constructions such as multiplicative cascades on wavelet coefficients [5] or Mandelbrot binomial cascades [41]. This remark makes explicit the link between multifractals and ideas that have already been applied to image processing [45, 55, 56]. Infinitely Divisible Cascades (IDC) are a family of multifractal processes first introduced in [1, 4, 13, 42, 48] and recently proposed in [12] to model the statistics of natural images. Our approach uses a sub-family of IDC, namely Compound Poisson Cascades (CPC), which permit the construction of multifractal processes featuring the main statistical properties of natural images, including higher order correlations.

2.3 Compound Poisson cascades (CPC)

In this section, we recall the main definitions and properties of compound Poisson cascades (CPC), a subfamily of infinitely divisible cascades. CPC were first introduced by Barral & Mandelbrot (2001) [4] as Multifractal Products of Cylindrical Pulses and later generalized to infinitely divisible cascades by several authors. We refer to [1,11,12,14,15, 42,48] for more detailed presentations of infinitely divisible cascades in general.

This model is based on a multiplicative construction where smaller scales of an image inherit information from larger scales in a continuous way. Let $Q_\ell^L(\mathbf{x})$ be the pixel value at location $\mathbf{x}$; let L and ℓ, $L > \ell$, the limiting largest and smallest scales of the resulting image. Let $(\mathbf{x}_i, r_i)$ a Poisson point process with: (i) $\mathbf{x}_i$ i.i.d. uniformly distributed in the 2D plane, ensuring the homogeneity of Q_ℓ^L in space; (ii) $\ell \leq r_i \leq L$ independent of $\mathbf{x}_i$ and i.i.d. with density $1/r^3$ (so that the final texture is mathematically well defined if $\ell > 0$ only). The $(\mathbf{x}_i, r_i)$ are marked by i.i.d. positive random variables W_i called multipliers, independent of the $(\mathbf{x}_i, r_i)$. For all $\mathbf{x}$ of the image, the CPC $Q_\ell^L(\mathbf{x})$ is defined by

$$Q_\ell^L(\mathbf{x}) = \frac{\prod_i W_i^{\mathbb{1}_{\mathscr{D}(\mathbf{x}_i,r_i)}(\mathbf{x})}}{\mathbb{E}\left[\prod_i W_i^{\mathbb{1}_{\mathscr{D}(\mathbf{x}_i,r_i)}(\mathbf{x})}\right]} \tag{10}$$

where $\mathbb{1}_{\mathscr{D}(\mathbf{x}_i,r_i)}$ is the characteristic function of the disk of radius r_i centered in $\mathbf{x}_i$ and the normalization ensures $\mathbb{E}Q_\ell^L = 1$.

Such models are homogeneous but very irregular objects and correspond from a mathematical standpoint to *distributions* with log compound Poisson law. They can be seen as densities of multifractal measures. Indeed, in the limit $\ell \to 0$, the compound Poisson cascade tends to zero almost everywhere (see [4, 14, 42] for a complete presentation of their mathematical properties). From a mathematical standpoint, the object of study would be the measure associated to a CPC. A CPC can be seen as the density of a measure, just like a distribution. As a consequence, even though the CPC tends to zero almost everywhere (think of a Dirac distribution for instance), the corresponding measure may not be

zero everywhere ; the measure is then said to be non degenerate (in the limit $\ell \to 0$). The scale invariance of a CPC is characterized by $H = 0$ and $\tau(q) = q(\mathbb{E}W_i^q - 1) + 1 - \mathbb{E}W_i^q$ for scales between ℓ and L. This means that the choice of the distribution of the multipliers W_i determines the scale invariance properties of a CPC. Their Fourier spectrum obeys a power law $\propto 1/k^{2+\tau(2)}$ ($\tau(2) < 0$). By construction, $Q_\ell^L(\mathbf{x})$ is equal in distribution to $Q_{\ell/L}^1(\mathbf{x}/L)$. Its variance is given by:

$$\mathrm{var}(Q_\ell^L) = (\ell/L)^{\tau(2)} - 1 \tag{11}$$

Let $f(\mathbf{x})$ a geometric kernel defined by a non negative function with compact support. A natural generalization of the previous definition is

$$Q_\ell^L(\mathbf{x}) = \frac{\prod_i W_i^{f\left(\frac{\mathbf{x}-\mathbf{x}_i}{r_i}\right)}}{\mathbb{E}\left[\prod_i W_i^{f\left(\frac{\mathbf{x}-\mathbf{x}_i}{r_i}\right)}\right]} \tag{12}$$

Note that CPC connect to other existing models of natural images. For instance, taking the logarithm of eq. (12), one gets

$$\log Q_\ell^L(\mathbf{x}) = \sum_i \log W_i \cdot f\left(\frac{\mathbf{x}-\mathbf{x}_i}{r_i}\right) + K \tag{13}$$

which looks much like the Transported Generator Model by Grenander & Srivastava (2001) [25] or the learnt sparse codes by Olshausen & Field (1996) [44].

An essential property of CPC is that for any $0 < r_2 \leq r_1 \leq r_0$, $Q_{r_2}^{r_0}$ obeys a multiplicative multiscaling decomposition

$$Q_{r_2}^{r_0} = Q_{r_1}^{r_0} \cdot Q_{r_2}^{r_1} \tag{14}$$

where $Q_{r_1}^{r_0}$ and $Q_{r_2}^{r_1}$ are two independent CPC with the same $\tau(q)$. This essential property is the core of the approach presented in this article.

The fractional pseudo-integration, denoted by the operator $\mathscr{I}_H$, is performed in practice by a $1/||k||^H$ low-pass filter in the Fourier domain for $||k|| > 0$ (the singularity at $k = 0$ is treated separately). The fractional pseudo-derivation denoted by $\mathscr{D}_H$ is the inverse of the integration and is performed in practice by a $||k||^H$ high-pass filter. These operations preserve scale invariance but modify the scaling exponents $\zeta(q)$ by adding, respectively subtracting, a linear part qH, see Corollary 1 in [31]. Thus, CPC may be used to model very rough images (or textures) with $\zeta(1) = 0$ as well as smoother images with $\zeta(1) = H > 0$.

In terms of functional analysis, we recall [32] that the set of multiscaling exponents $\zeta(q)$ characterizes the collection of Sobolev and Besov spaces to which a function X belongs since $\zeta(q) = \sup\{s : X \in B_p^{s/p,\infty}\}$. Note that Besov spaces express in a precise statement how sparse an image is in the wavelet domain. A multifractal function X belongs to the Sobolev space $L^{1,\zeta(1)}$ and to Besov space $B_1^{\zeta(1),\infty}$. The construction of CPC imposes that $\zeta(q) = \tau(q)$ and $\zeta(1) = \tau(1) = 0$ while images considered here may be more regular with $\zeta(1) = H > 0$. Bare CPC are quite singular.

3 Virtual scale invariant super resolution

This section describes how the CPC presented above can be used to propose a virtual scale invariant super resolution procedure. First we state the problem again and precise which desirable properties such a procedure should obey.

3.1 The approach

Our purpose is to virtually refine the resolution of scale invariant textured images thanks to an adapted augmentation of information. We require the augmentation to obey both *statistical* and *physical consistency* with the initial image. By *statistical consistency* we mean that the resulting image should have the same scale invariance properties as the original one, see figure 2. More precisely, the spectrum of the super resolved image should correspond to a power law extrapolation of the initial spectrum towards higher frequencies, see fig. 2(a). Moreover, the higher order correlations described by the multiscaling exponents $\zeta(q)$ should also be extrapolated to scales smaller than the initial pixel size, see fig. 2(b). By *physical consistency*, we mean energy conservation. Zooming out the magnified image to the initial resolution should yield the initial image back, see figure 2. To this aim, one must add details with well suited properties at scales below the pixel size of the original image.

Some existing methods [3, 16, 26, 28, 37] aim at preserving scale invariance but they are deterministic and do not extrapolate the multifractal behavior of the initial image. Our method is more flexible since it adds scale invariant and multifractal information at higher resolution in a stochastic manner. However it must be noticed that a fundamental assumption which is also a limitation is that the scale invariance properties of the original image are known, which is the case for, e.g., synthetic textures, or images that have been previously analyzed. The initial image is supposed to have some random texture looking, e.g. taken from a turbulent physical system such as the quiet Sun characterized by the scale invariance parameters H and $\tau(q)$ estimated from a prior multifractal analysis [18].

The main thrust is to a priori describe the initial image by the following *global* model:

$$I_1 = I_0 + \alpha \mathscr{I}_H\{Q_{r_1}^{r_0} - \langle Q_{r_1}^{r_0} \rangle\} \tag{15}$$

where $\langle\rangle$ stands for spatial averaging and I_0 for the average intensity of the image. The fluctuation term is a fractionally

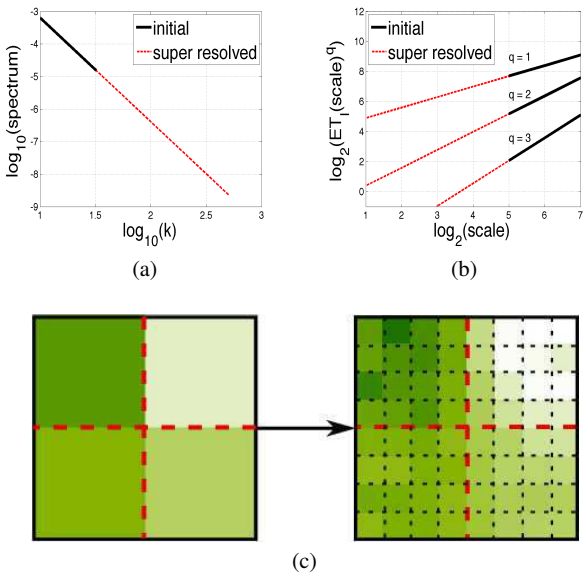

Fig. 2 (a)&(b) Statistical consistency: we aim at a super resolution procedure which will add subpixel details by extrapolating the power law spectrum as well as higher order scale invariant properties with the same multiscaling exponents $\zeta(q)$ of the original image.(c) Physical consistency: the super resolution procedure should obey the energy conservation rule. The sum of intensities of subpixels of a given macropixel must be equal to the intensity of this macropixel.

pseudo-integrated CPC with zero mean ($\mathscr{I}_H$ is a $1/||k||^H$ low-pass filter in the Fourier domain), amplified by a factor α. The scales r_0 and r_1 stand for the largest scale and the finest scale (the pixel size) of the image. We stress that this *global* model is not really aimed at describing the complete image but is only used to derive a *local* procedure of augmentation. Recall that the scale invariance properties of such an image are characterized by $\zeta(q) = qH + \tau(q)$.

We derive a *local* procedure to add random correlated details in every pixel of the initial image thanks to the multiscale multiplicative decomposition property of CPC, see eq.(14). The main idea of this magnification procedure is to replace $Q_{r_1}^{r_0}$ by $Q_{r_2}^{r_0}$ in (15) to get an image I_2 at resolution $r_2 < r_1$. The procedure is schematically represented in fig. 3. Eventually, a renormalization step ensures that the procedure is conservative in the sense that zooming out to the initial resolution gives the original image back.

The idea of considering a physical quantity as some fractional integral of a density that is an intensive quantity is not new. Our model is quite similar to those used by physicists to describe measurements from turbulent flows. For instance, one may think of the fractional fields by Schertzer & Lovejoy (1987) [47]. The underlying intuition is that physical measurements are averages of some local density over some spatial or temporal domain. Here, the CPC $Q_{r_0}^{r_1}$ plays the role of a density which may exhibit a very singular behavior, similar to that of a distribution. The image is the result of the counting of photons emitted by some region of space and transmitted through a propagation medium. Therefore, one may consider the intensity of an image as a kind of average over a spatio-temporal domain. The model described by (15) fits to this phenomenology by producing a scale invariant image as a fractional integral (which preserves scale invariance) of some scale invariant density distribution.

3.2 Super resolution procedure

This section describes in detail the elementary steps of our procedure. As a first step, we need to magnify and resample the original image I_1 at resolution $r_2 < r_1$. To this aim, we use a spline interpolation [53] leading to a smoothed version I_{interp} of I_1 with minimum addition of information. Indeed, spline interpolation has been shown to be very effective to this purpose. From a mathematical standpoint, the image I_{interp} may be quite regular and not comparable to a singular distribution such as a CPC. Frequencies corresponding to scales below r_1 are cut off in I_{interp} whereas a $\propto k^{-(2+2H+\tau(2))}$ spectrum is wanted. An adapted fractional derivation of order $H = \zeta(1)$ yields the intermediate image

$$J_1 = \mathscr{D}_H I_{interp} \quad \longleftrightarrow \quad \alpha\left(Q_{r_1}^{r_0} - \langle Q_{r_1}^{r_0}\rangle\right) \text{ in (15).} \tag{16}$$

In some sense, this fractional derivation brings J_1 down to the same class of regularity as a CPC. Next step consists in using the multiscale decomposition (14) of CPC to replace J_1 by

$$\begin{aligned} J_2 &= \alpha\left(Q_{r_2}^{r_0} - \langle Q_{r_2}^{r_0}\rangle\right) \\ &= J_1 \cdot Q_{r_2}^{r_1} + \alpha\langle Q_{r_1}^{r_0}\rangle\left(Q_{r_2}^{r_1} - \langle Q_{r_2}^{r_1}\rangle\right) \end{aligned} \tag{17}$$

where the term $Q_{r_2}^{r_1}$ contains the new information at scales smaller than r_1. This image J_2 contains new details down to resolution $r_2 < r_1$. Note that $Q_{r_2}^{r_1}$ is independent of $Q_{r_1}^{r_0}$; it is generated using (10) with the same parameters as $Q_{r_1}^{r_0}$. Since $Q_{r_2}^{r_1}(\mathbf{x}) \overset{d}{=} Q_{r_2/r_1}^{1}(\mathbf{x}/r_1)$, the information brought by the CPC between scales r_1 and r_2 depends on the magnification factor r_1/r_2 only. The first term in (17) mainly describes the augmentation of information in J_1 at scales $r_2 \le r \le r_1$. It ensures the coupling between the initial image J_1 and the new details $Q_{r_2}^{r_1}$. The second term in some sense ensures that the energy level of the new details is consistent with the initial image. J_2 is then expected to be characterized by the same $\tau(q)$ as I_1 and the same power law Fourier spectrum over a larger range of spatial frequencies. Note that each realization of $Q_{r_2}^{r_1}$ will produce one possible realization of the magnification of the original image among a potential infinity since we use a kind of stochastic extrapolation, see figure 4.

At this stage, the parameter α plays an important role since it controls the weight of the new small scale details. Assuming that the proposed model (15) holds, it depends on

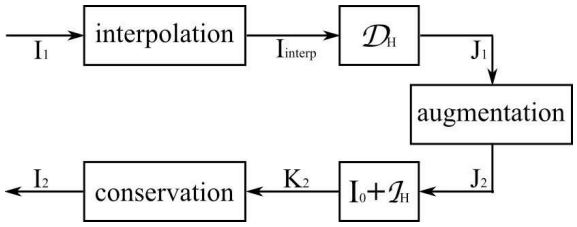

Fig. 3 Schematic view of the magnification process.

the variance of J_1, the initial scale range r_1/r_0, and on $\tau(2)$. It can be estimated using (11):

$$\widehat{\alpha} = \sqrt{\frac{\widehat{\mathrm{var}(J_1)}}{\widehat{(r_1/r_0)}^{\tau(2)}} - 1} \tag{18}$$

where $\tau(2)$ can be estimated from the power law Fourier spectrum $\propto 1/k^{2+2H+\tau(2)}$ or from some multiscaling analysis. Some problem may rise from an inaccurate estimate of α. Section 4.1.3 details the sensitivity of the present approach to parameter estimates and shows that no critical problem appears.

The pseudo-integration step yields

$$K_2 = I_0 + \mathscr{I}_H J_2 \tag{19}$$

At this stage, we must comment on the physical meaning of K_2. Since K_2 should be interpreted as a light intensity, it is expected to be a non negative quantity. In fact, there is some uncertainty on the positiveness of K_2 since we cannot ensure that the fractional integration operator will not yield values $\mathscr{I}_H J_2 < -I_0$. However, we have observed on real images (quiet Sun images from EIT onboard SoHo for instance) that this condition was well obeyed with high probability. Negative values appear to be isolated and may reasonably be considered as outliers, even though they tell us that the model may not be exact and remains an approximation. In practice, one needs to check for positiveness of K_2 and to force negative values to zero.

Finally, the magnified image I_2 results from a renormalization of K_2 which makes the procedure "energy conservative". While (17) adds information at scales $r_2 \le r \le r_1$, it also slightly affects scales larger than r_1 as well and the desirable energy conservation rule is not obeyed. Therefore, we impose that the sum of intensities in regions of I_2 corresponding to a pixel of size r_1 in I_1 equals the pixel value in I_1.

The multiplicative augmentation procedure and the energy conservation step are non-linear and local operations so that they do not commute. As a consequence, a direct $\times 32$ magnification is actually different from five successive $\times 2$ magnifications. Ideally, the ratio r_2/r_1 should be close to 1 to carry out a continuous super resolution process. This is also important to preserve the scale invariance of the original image and to limit any "blocking" artifact due to the conservation step. In the present work, and for obvious practical reasons, we use $r_2/r_1 = 1/2$.

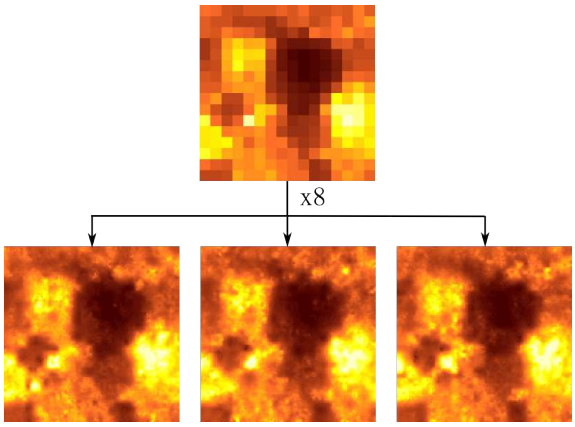

Fig. 4 Several realizations of possible virtually super resolved versions of the same low-resolution initial image. The general aspect is quite similar while local details vary from a realization to the other.

4 Illustration

4.1 Synthetic examples

We illustrate our approach in the ideal case where the initial image is precisely of the form given by (15). A set of initial images of size 32×32 is built with $\alpha = 8$ and $I_0 = 23$, for $r_0 = 1$ and $r_1 = 1/32$ and with $H = 0.7$. In these examples we have chosen $\tau(q) = -((1+T)^q/(1+qT) - 1)$ where $T = 0.7$ which leads to $\tau(2) = -0.20$. The expected Fourier spectrum is therefore of the form $1/k^{3.2}$. A magnification $\times 32$ is performed as five '$\times 2$' elementary magnifications leading to 1024×1024 images. This corresponds to a distribution of the multipliers in (10) proportional to $W^{1/T-1}$ for $W \in [0, 1+T]$ with $\mathbb{E}W = 1$; the choice $T = 1$ would correspond to multipliers with uniform distribution in $[0,2]$.

4.1.1 Visual aspect

Fig. 5 compares typical results obtained by simple interpolation (with no augmentation of information) by using cubic B-spline as described in [53] with those obtained from the magnification procedure described above (see our webpages for other examples). Here, we assume that α, r_1/r_0 and $\tau(2)$ are exactly known. Fig. 5 clearly illustrates the augmentation of information by the introduction of new small scale details inside initial pixels while a simple interpolation only smoothes the image. Moreover, lowering (by aggregation) the resolution of I_2 back to r_1 yields I_1 back: the energy conservation rule is obeyed. At least on purely visual grounds,

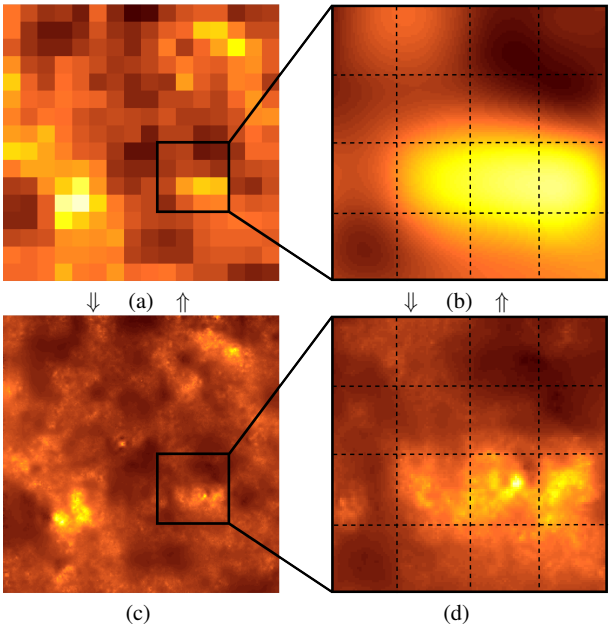

Fig. 5 Illustration of our magnification procedure: (a) initial 16×16 image, (b) zoom in the ×32 interpolated image contained in the 4×4 black square of the initial image; cubic B-spline interpolation was used [53], (c) ×32 magnified image with augmentation, (d) zoom in the black square region. The dotted lines corresponds to initial pixels.

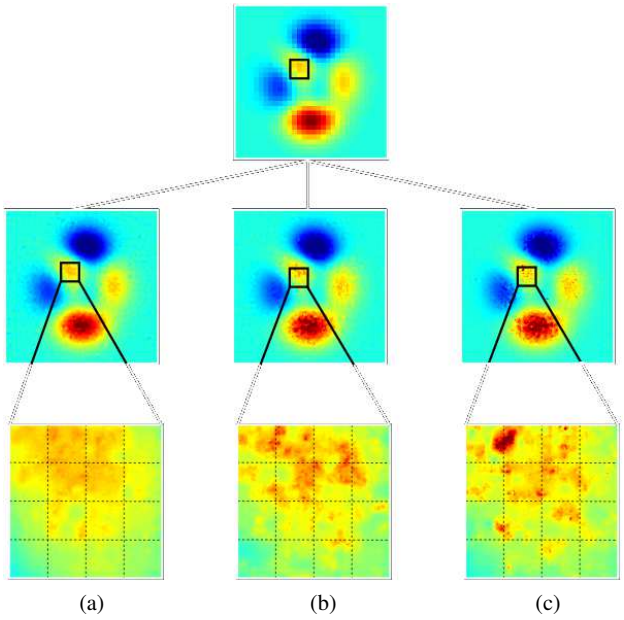

Fig. 6 Comparison between results obtained from the same original regular image (peaks of Matlab) by using a CPC (a) slightly, (b) mildly, (c) strongly multifractal. Dashed lines corresponds to the initial pixels.

the image on fig. 5(c) appears as a relevant candidate to describe plausible details that may be underlying the image on fig. 5(a) (idem for fig. 5(d) and (b)). Next section will show that this "plausibility" is essentially due to the statistical and physical consistency of the added small scale details.

The choice of the precise multifractal model underlying a CPC based super-resolution is crucial. Fig. 6 shows results obtained from the same initial image for slightly, mildly and strongly multifractal models. The visual consequences are clear: the more multifractal the model, the more intermittent and disordered the texture. While fig. 6(a) is only slightly different from some usual regular interpolation, fig. 6(b) and (c) exhibit more localized "extreme" events. Again, the visual aspect betrays statistical properties. Note again that a potentially infinite number of images may be underlying some given initial low resolution image. We emphasize again that we do not predict some deterministic hidden information but we only propose a class of plausible underlying high resolution images, see fig. 4.

4.1.2 Scale invariance properties

Fig. 7(a) presents a log-log plot of the Fourier spectra of the original image I_1 and of the virtually super resolved image I_2 after magnifications by factors 2 and 32. These spectra result from averaging over all possible directions. We see that the power law Fourier spectrum of I_1 has been preserved at lower frequencies and extended to higher frequencies with the same exponent and without any discontinuity. This illustrates the fact that both the energy content and the energy level of the added small scale/high frequency details are consistent with those of the initial image. The scale invariant behavior of second order correlations has been correctly extrapolated to high frequencies.

To be even more precise, we now turn to higher order correlations which are described by the multiscaling behavior of absolute moments of wavelet coefficients, see eq. (4). Fig. 7(b) shows that this multiscaling behavior is indeed well extrapolated to smaller scales since the linear behavior in a log-log plot has been extended over a wide range of octaves at smaller scales. Fig. 7(c) shows that the associated multiscaling exponents estimated from I_2 are close to the expected ones within reasonable error bars.

Finally, we comment on the evolution of the histograms of wavelet coefficients. As explained in section 2.2 thanks to eq. (8), the multiscaling behavior we just mentioned is closely linked to the evolution of the histograms of wavelet coefficients through scales. This evolution usually goes from nearly Gaussian at larger scales to less and less Gaussian (for instance, generalized exponential) distributions at smaller scales. This is often called the *intermittency phenomenon* by physicists in turbulence. Indeed, this departure from the normal law at small scales means that extreme events happen 'abnormally' often at small scales. These extreme events are associated to high dissipation regions in fluid flows. In images, they are rather associated to localized large gradient areas like isolated bright points or edges. Fig. 8 shows

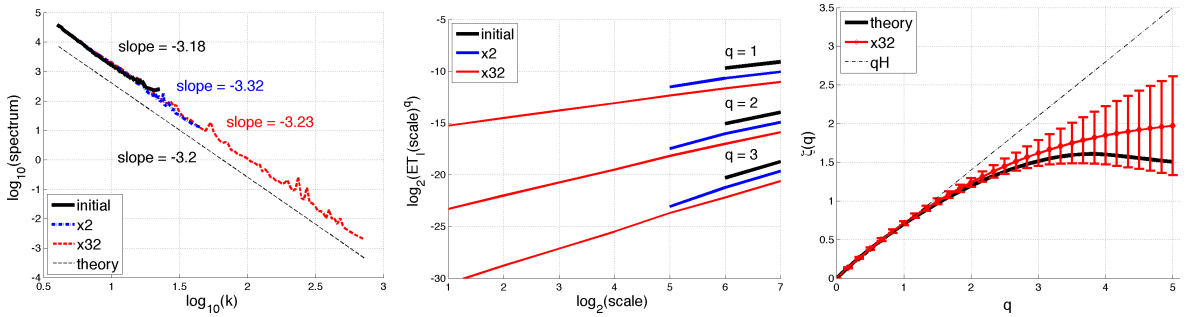

Fig. 7 (a) Power law Fourier spectra; (b) multiscaling behavior of the absolute moments of wavelet coefficients of order 1, 2 and 3 of $\times 2$ and $\times 32$ magnified images; (c) multifractal exponents of magnified images.

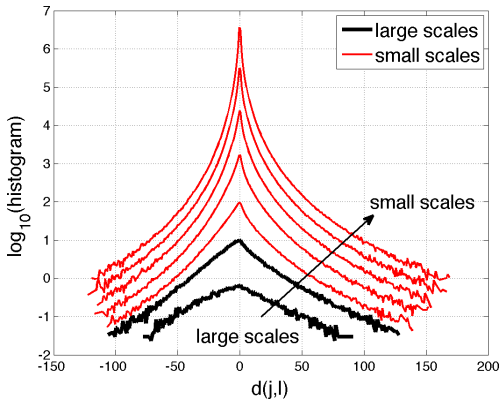

Fig. 8 The evolution of the histograms of wavelet coefficients for octaves available from original images (in black) towards less and less Gaussian distributions for the augmented images where new octaves are reachable.

the histograms of wavelet coefficients at smaller and smaller scales from bottom to top. In log-scale, a Gaussian distribution would be associated to a parabola, while here the histograms are more and more peaked and heavy tailed as smaller scales are considered. This is consistent with the well known fact that generalized exponentials are usually good candidates to model wavelet coefficients distributions of natural images.

Thus we have shown, at least through these numerical experiments, that our magnification procedure adds new information to the original image while (i) enhancing its visual aspect, (ii) preserving its scale invariance properties and (iii) being conservative with respect to zoom in and out operations. These experiments have been applied to a wide variety of multifractal images and have given similar results.

4.1.3 Sensitivity to parameter estimates

In this work, we always assume that the scaling exponents of I_1 are known from a prior analysis. In practice, we assume for instance that these images belong to some class of textured images such as quiet Sun images [18]. Therefore, a multifractal analysis can be performed prior to this super resolution procedure. Estimates of the multiscaling exponents $\zeta(q)$ are then known. A parametric model among those CPC that can be simulated is chosen to reproduce the same multiscaling properties as faithfully as possible. An important limitation of this method is its dependence on the precision of $\zeta(q)$ estimates which require a large amount of data. Another limitation roots in the use of parametric models. There is some work left to find an approach which could deal with a single image.

While all parameters have been assumed to be known above, we now consider the more realistic situation where α and the ratio r_1/r_0 are unknown. As seen in (18), α depends on r_1/r_0, the ratio between the initial resolution r_1 and the largest scale r_0 present in the image. An error on the estimate $\widehat{r_1/r_0}$ may lead to an error on the estimate $\widehat{\alpha}$, see eq. (18). The scale r_1 is known a priori since it is the smallest scale available, the pixel size. Therefore, the estimation of α is directly linked to the estimation of the larger scale r_0 in the image. It may be in general smaller but sometimes larger than the image size; in any case, this quantity is difficult to estimate accurately. One must check whether an error on this estimate could have quantitative or qualitative consequences. In the case where r_0 is overestimated, α is underestimated so that the power of details is too small: the final image misses some energy at high frequencies to accurately extend scale invariance properties into the range of scales $[r_2, r1]$, see fig. 9(a)&(d). However, remark that the Fourier spectrum does not fall down dramatically. There is only a small fall off at the frequency corresponding to the scale r_1 which is not so easy to detect by simply looking at the image. This is expected when looking closer at eq. (17): the procedure adds small scale details, even when $\hat{\alpha} = 0$. Note that if the true α was really zero, the initial image would be constant $I_1 = I_0$, and there would be no reason to use the present procedure. The use of eq. (17) is relevant under the assumption that $\alpha \neq 0$ only. In the case where r_0 is under-

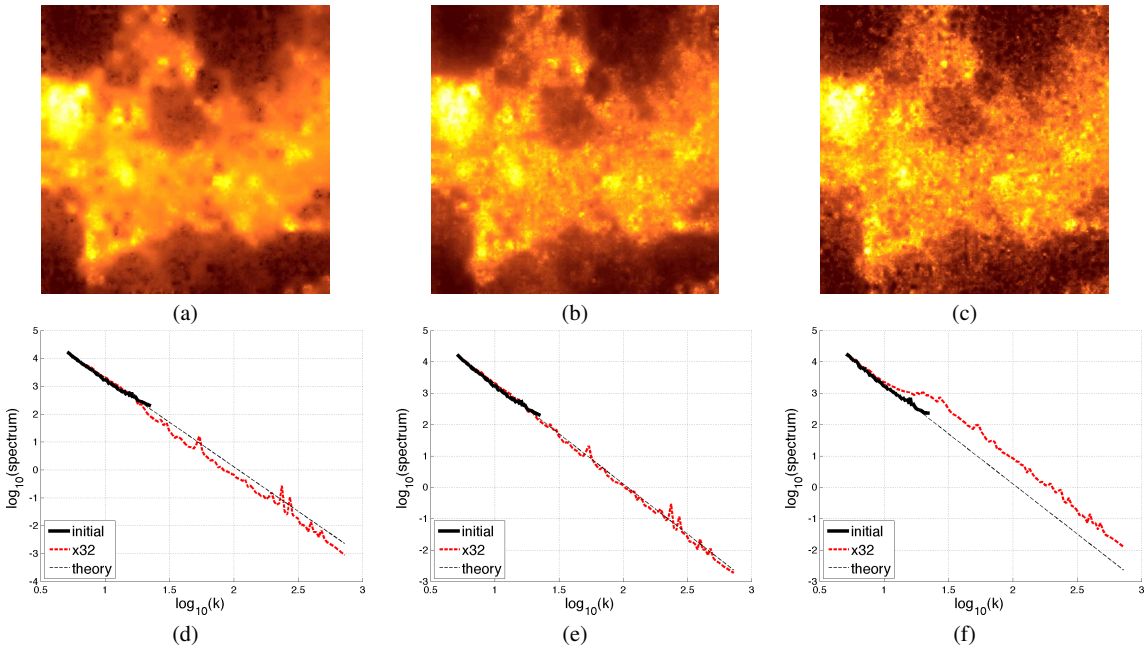

Fig. 9 Illustration of the consequences of an error on the estimate of r_0 and α. First row: images resulting from a $\times 32$ magnification; second row: corresponding Fourier spectrum averaged over all directions. (a)&(d) when α is underestimated; (b)&(e) when α is correctly estimated; (c)&(f) when α is overestimated.

estimated, the power of details is too big and results in too much energy at high frequencies, see fig. 9(c)&(f). Again, scale invariance is not correctly extended to smaller scales; even more, this would give rise to clear visual artifacts since blocks of approximate size r_1/r_2 could appear in the super resolved image. In the limit where $\hat{\alpha}$ is really too large, the super resolved image would even look noisy, in particular at scales between r_2 and r_1.

Fortunately, a precise estimation of r_0 is not so crucial for the procedure to remain efficient. For instance, let us consider that r_0 will be often close to Nr_1 (r_1 = pixel size) for an $N \times N$ image so that $\widehat{r_1/r_0}$ can be replaced by $1/N$. In the present example, $\tau(2) = -0.20$, $r_0/r_1 = 1/32$ and $\alpha = 8$ (here $\mathrm{var}(J_1) \simeq 66$). If the estimation of r_0 is $\widehat{r_0} = 2 \times r_0$ (respectively $\widehat{r_0} = r_0/2$), $\widehat{\alpha} = 7.02$ (respectively $\widehat{\alpha} = 9.3$) instead of $\alpha = 8$. In other words, a factor 2 on $\widehat{r_0}$ leads to a 14% uncertainty on $\widehat{\alpha}$. Fig. 10 shows the relative error on $\hat{\alpha}$ as a function of the relative error on $\widehat{r_0}$. Furthermore, the fractional pseudointegration consists of a lowpass filtering which makes this uncertainty even smaller; the conservation step tends to reduce it as well. In the end, the error is close to negligible. Note that $\widehat{\alpha} = \alpha/2$, respectively $\widehat{\alpha} = 2 \times \alpha$, would correspond to $\widehat{r_0} = 93.4$, respectively $\widehat{r_0} = 0.09$ instead of $r_0 = 1$. In other words, an error of a factor between 10 and 100 on $\widehat{r_0}$ would be necessary to yield an error of a factor 2 on $\widehat{\alpha}$. Let us remark that the sensitivity of α estimate to r_0 also depends on the global regularity of the original image (larger $|\tau(2)|$ will degrade the estimation precision over α). However, we studied the typical case $\tau(2) = -0.20$ which already corresponds to rather irregular images and gives good hints to what will likely happen in usual situations.

In summary, the maximum error on r_0 is expected to be within a factor 2 which leads to an error on α of the order of 10%. Furthermore, the fractional pseudo-integration as well as the conservation step tend to reduce the consequences of this uncertainty on $\widehat{\alpha}$. In the end, the error is close to negligible. As a conclusion, the accuracy of the estimation of r_1/r_0 and α is not critical.

Another possible source of error which is easier to deal with may be the estimate of the variance J_1 in (18). Indeed, if the initial image is to small, very few statistics are available to estimate $\mathrm{var}(J_1)$ so that α will be poorly estimated. One must take care of working either with one sufficiently large initial image or with a set of a sufficiently large number of images to get an accurate estimate $\widehat{\mathrm{var}(J_1)}$.

4.1.4 Extrapolation of histograms

One important initial motivation of this work is the questions asked by solar physicists about their future high resolution observations. Among others, two questions are simple to formulate: knowing present low resolution images from E.I.T (1 pixel = 1800 km), can we have a reasonable idea of what would images at a resolution 25 times smaller (1 pixel = 80 km) look like ? and how far could these new images be underexposed ? Indeed, the photon flux measured

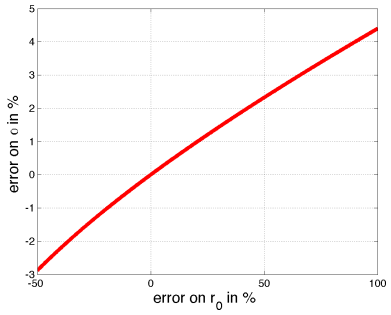

Fig. 10 Relative error (in %) on α as a function of the relative error (in %) on the estimate of r_0.

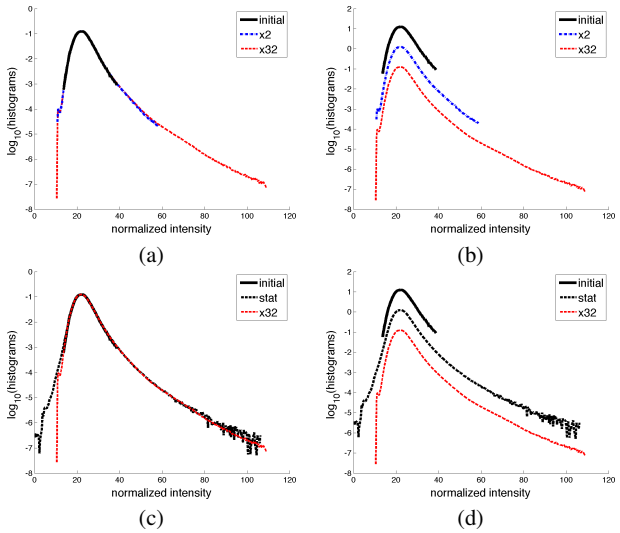

Fig. 11 (a) & (b) Histograms of the initial 32x32 image and of corresponding virtually super resolved versions for enlargement factors x2 to x32. (c) & (d) Comparison between histograms of intensity estimated from data sets of 32x32 and 1024x1024 images using identical statistics: even the tails are quite similar. Normalized intensity is the intensity times the square of the enlargement factor; on figure (b) & (d) the graphs have been artificially translated for sake of clarity.

by one pixel of the sensor decreases with the resolution. The virtual super resolution procedure we presented above proposes a method to give a plausible answer to the first question. Moreover, this approach gives an answer to the second one as well. Since we are directly aiming at the modeling of the physical light intensity in a quantitative manner, we expect that the histograms of the virtually super resolved images can be estimated. This will permit us to study the necessary characteristic of the data acquisition system to ensure that images be sufficiently exposed to be usable. Here we illustrate this possibility on simulated images first. The application to quiet Sun images will be evoked in next section. We consider the same numerical experiments as in previous sections.

Fig. 11(a)&(b) show the histograms of initial images of size 32×32 obtained from fractionally integrated CPC with the parameters defined at the beginning of section 4.1. This figure also shows the histograms of corresponding virtually super resolved versions for enlargement factors $\times2$ and $\times32$. At first sight, we have in some sense implicitly extrapolated the histograms of the initial low resolution images. The mode of the histogram corresponding to the initial images is preserved in high resolution images. This observation calls for several comments. The multifractal behavior is linked to the intermittency phenomenon evoked earlier which gives rise to abnormally frequent extreme events at small scales (again abnormal means more frequent than with a Gaussian distribution). Therefore one expects that the histograms of super resolved images have heavier tails than initial low resolution images. This is true for pure CPC (with no fractional integration). The finer the resolution of a CPC, the more frequent large isolated values are. Here, on images which correspond to fractionally integrated CPC, the result is apparently the same. The histogram of the magnified image has a larger tail at large intensities than original images. However, let us remark that we are comparing histograms estimated from datasets of different sizes: super resolved images contain $32^2 = 1024$ times more points than the original dataset. Due to a simple statistical effect, the tail of the histogram of magnified images is necessarily better estimated. To be able to distinguish the result of the super resolution procedure from purely statistical effects, one must compare histograms estimated on datasets of identical sizes.

Fig. 11(c)&(d) compare the histogram of intensity estimated from a set of $N\times1024$ images of size 32×32 to the histogram estimated from N images enlarged 32 times. The surprising result is that both histograms are very similar. The pure statistical effect is far from negligible ! It appears that the fractional integration step plays a crucial role here. Indeed, we have repeated the same experiment for various values of H between 0 and 1. For small values of H, say smaller than 0.5 ($H = 0$ means that we consider a pure CPC), one can observe some real difference between the histogram of super resolved images and that of original (low resolution) images. This is consistent with our intuition of multifractality. For large values of H, say greater than 0.5, the histogram of super resolved images is quite similar to that of low resolution initial images if comparable statistics are used for estimation. The larger H, the closer the histograms. Our intuition is that this may be due to some kind of 'Central Limit Theorem' effect since fractional integration is equivalent to some low pass filtering which sums a large number of (non independent) random variables. Indeed, we observe that, for sufficiently large H, the histogram of super resolved images is close to some distribution which may be independent of the enlargement factor.

In practice only a limited number of images is available. The super resolution procedure will then provide us both with virtually super resolved images and with a tool

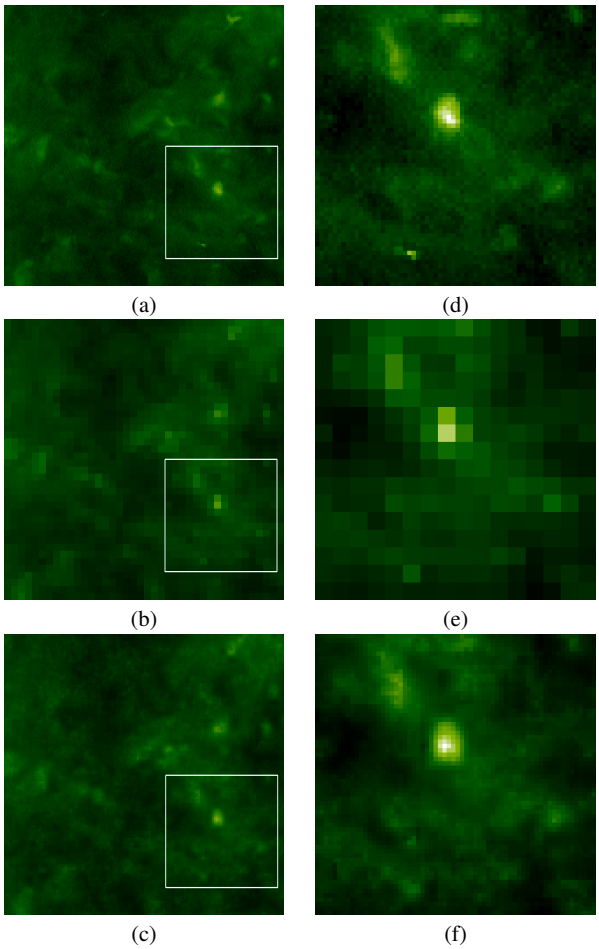

Fig. 12 Application of our CPC based super-resolution on a coarsened version of some quiet Sun image : (a) initial image at full available resolution, (b) image coarsened by a factor 4 (pixels have been grouped within 4×4 blocks), (c) image obtained by CPC based super-resolution $\times 4$. Fig. (d), (e) & (f) are zooms in the same (white square) region of (a), (b) & (c) respectively.

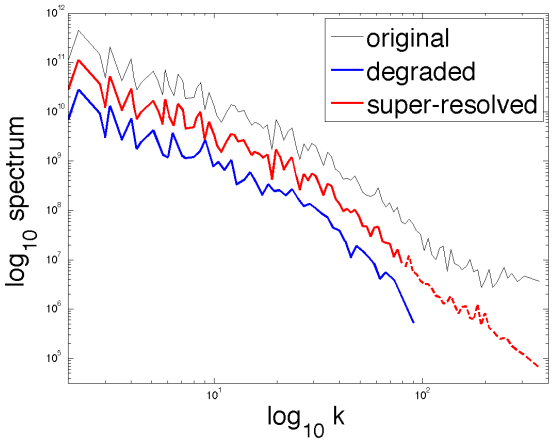

Fig. 13 Fourier spectra averaged over all directions for: an original quiet Sun image; at artificially degraded $(1/4)$ resolution; $\times 4$ super-resolved image obtained from the degraded image. Spectra have been artificially translated for sake of clarity of the presentation.

to extrapolate various statistical quantities at high resolution (like histograms of intensity or wavelet coefficients...). As observed above, a careful numerical study shows that these extrapolations are consistent with what one would expect by taking into account the multifractal nature of considered images.

4.2 Application to quiet Sun images in the extreme UV

4.2.1 Results

This work originates from questions asked by astrophysicists and solar physicists in particular. In many cases and despite constant progress of instrumentation, the smallest physical scales remain out of reach of observation. Astrophysicists deal with remote sensing of complex objects. These huge objects contain structure over an incredibly large range of scales, so that we may never access a fully detailed knowledge of them. Moreover, the finest observations are now provided by telescopes onboard spatial missions. As a consequence, the whole embedded apparatus must be well dimensioned and validated before launch. Such a requirement calls for some relevant data sets to test the whole system in as realistic conditions as possible. To answer at least part of the questions, the present virtual super resolution procedure appears as a very interesting tool. Indeed, statistical consistency is physically grounded in the current state of knowledge. The resulting images are physically credible and can be used to study various aspect of the necessary image processing. Fig. 12 compares the ground truth of some quiet Sun image at the available resolution with the result of our procedure applied to a coarsened version (resolution has been artificially degraded by a factor 4). The textural aspect of the image is satisfactorily recovered even though there are differences at small scales between the ground truth and the virtually super-resolved image. Recall that these differences are expected. Moreover, fig. 13 shows that the Fourier spectrum is indeed well extrapolated at high frequencies. The slight discrepancy between the extrapolated spectrum and the original one is expected and essentially roots in the presence of Poisson noise in the original image. This noise is partly suppressed by the coarsening (low-pass) procedure used to artificially degrade the resolution. In principle, the super-resolved image should be compared to the perfectly Poisson denoised original image, which incidentally enlightens the importance of Poisson denoising for such an approach.

For comparison, fig. 14 shows the results obtained for some part of an image of the quiet Sun by using either the *new edge directed interpolation* by Li & Orchard (2001) [39],

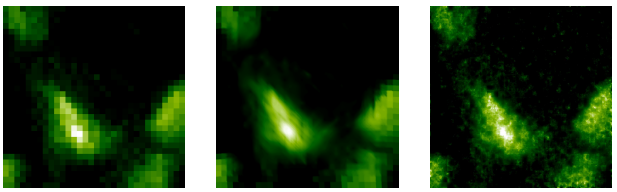

(a) (b) (c)

Fig. 14 Comparison between results obtained from the same original quiet Sun image (a) by applying a $\times 32$ magnification with (b) edge directed interpolation by Li & Orchard (2001) [39] and (c) our super-resolution method based on CPC.

fig. 14(b), or our method based on CPC, fig. 14(c). Edge directed interpolation is aimed at preserving local gradients, but does not add any small scale information as expected in a textured region. In contrast, our method may make edges a little irregular (but not blurry) and will add textured small scale details in a "plausible" manner.

4.2.2 Interest of the approach for quiet Sun images

Virtual super resolution could for instance help to optimize forthcoming embedded software for compression or denoising. Actually, images simulated by using a similar approach directly on the sphere are used to calibrate the future observations by Solar Orbiter [29]. One must keep in mind that usual compression algorithms usually assume that images are rather regular and that large scales dominate. As a consequence, they generally get rid of small scale details first. The rash use of any compression technique on (very expensive) high resolution images would lead to throw out most part of the expected benefit. Plausible simulated images are of great help to deal with such potential dilemma. Virtually super resolved images can also be used as a reference to study the effect of Poisson noise and to optimize denoising. As mentioned above, they also simply permit to estimate some statistical quantities of interest such as histograms of intensity which can help in predicting the level of exposition and thus an index of quality of future images. Fig. 15 shows the histograms obtained by using the present procedure on 54 E.I.T. quiet Sun images [18] provided by the Royal Observatory of Belgium. We will present this application in details elsewhere. A movie is available from our webpage at `www.isima.fr/~chainais/PUB/publications.html/quietSun_movie.avi` that illustrates a $\times 32$ zoom in a quiet Sun image. In the end, one low resolution pixel is replaced by $32 \times 32 = 1024$ high resolution pixels. Other illustrations are available from `www.isima.fr/~pchainai/PUB/ZOOM/zoom.html`

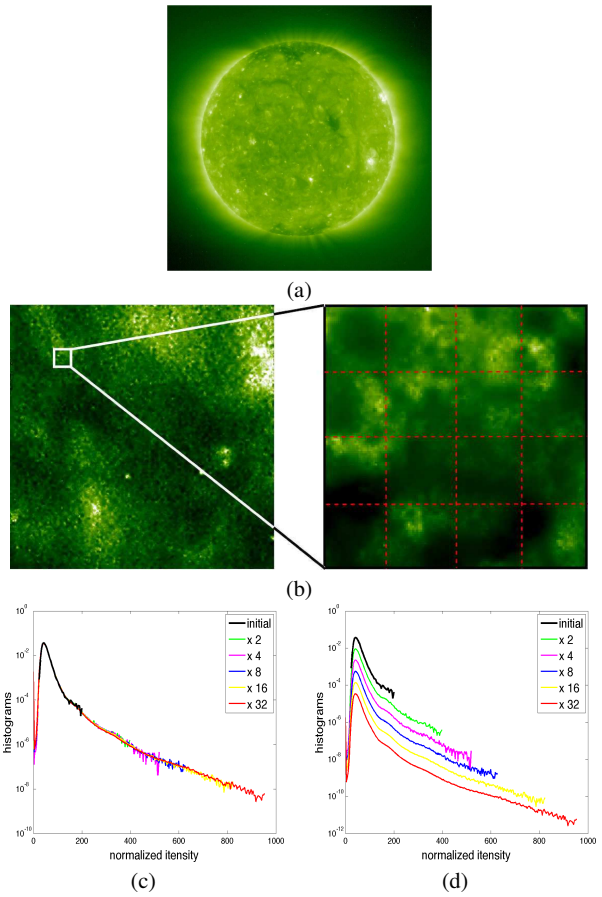

Fig. 15 (a) Example of an image of the quiet Sun in the extreme UV; (b) Illustration of the super resolution applied to a part of some EIT quiet Sun image. (bottom) Histograms estimated from 54 quiet Sun images and from corresponding virtually super resolved versions for various enlargement factors ranging from x2 to x32; (c) Histograms of normalized intensities; (d) the graphs have been artificially translated for sake of clarity.

5 Conclusion

Motivated by questions from astronomy and astrophysics, we have developed a virtual super resolution technique. This work originates in particular from the observation of quiet Sun images by E.I.T. onboard SoHo in the extreme UV [18] but could have applications to other remote sensing observations (clouds...). The main purpose is not to predict the true hidden high resolution information, but rather to propose a plausible prediction of what may be hidden at potentially any finer resolution than available. We are interested in textured (turbulent) images only. The present approach aims at using as little a priori as possible on the hidden information. It has been known for a long time that turbulent systems usually exhibit a scale invariant behavior [23]. This scale invariance often characterizes astrophysical objects where the range of physical scales at play is incredibly large compared to more usual terrestrial physical systems. As a conse-

quence, only a little part of this range of scales is available from observations which are limited and actually yield low resolution images. For instance, one pixel of the images of the Sun provided by the spatial telescope E.I.T. corresponds at best to a square of $(1800\ \mathrm{km})^2$ whereas physicists think that turbulence and therefore scale invariance might develop down to a scale of 100 m. The main thrust of our approach is to propose a plausible stochastic super resolution by only assuming statistical and physical consistency. Physical consistency simply means energy conservation: since we want to model light intensity, that is photon fluxes, the sum of the energies of high resolution subpixels must be the energy of the corresponding low resolution pixel. Statistical consistency means that virtually super resolved images should exhibit the same multifractal behavior as original low resolution images but over a larger range of scales. Basically, the Fourier spectrum of super resolved images must remain a power law spectrum at higher frequencies with the same exponent as original images. Moreover, we want that multiscaling (multifractal) properties be extrapolated as well. As a result, not only second order correlations are extrapolated but higher order ones as well.

This is made possible thanks to the use of fractionally integrated compound Poisson cascades, a family of multifractal stochastic processes with prescribed scale invariance properties. We have detailed our procedure to enlarge images with a potentially infinite factor. Thanks to numerical experiments we have shown that the result is visually quite satisfactory; moreover, the expected scale invariance multiscaling properties are indeed quantitatively well extrapolated at finer scales. This procedure opens the way to the prediction of some statistical quantities such as intensity histograms which can help to predict the exposition level of future observations. It also provides us with simulated images of forthcoming observations so that denoising, compression or detection algorithm can be studied and optimized before launching some spatial mission for instance. We have also evoked an application to quiet Sun images which will be presented in more details elsewhere. By the way, we mentioned that this approach assumes that multifractal properties are known which supposes the preliminary analysis of a sufficiently large set of images. This could be a limitation in some cases. An important direction for current and future work is the opportunity to adapt this method to a single image by directly identifying the underlying CPC structure thanks to optimization techniques for instance. Note that it can also be generalized to more than 2 dimensions, for the modeling of 3D structures such as clouds for instance.

The authors gratefully acknowledge anonymous referees for interesting and constructive remarks and suggestions.

References

1. Bacry, E., Muzy, J.: Log-infinitely divisible multifractal processes. Comm. in Math. Phys. **236**, 449–475 (2003)
2. Barnsley, M.: Fractal functions and interpolation. Constructive approximation **2**(1), 303–329 (1986)
3. Barnsley, M.: Fractals everywhere, second edition edn. Academic Press Professional (1993)
4. Barral, J., Mandelbrot, B.: Multiplicative products of cylindrical pulses. Probab. Theory Relat. Fields **124**, 409–430 (2002)
5. Benzi, R., Biferale, L., Crisanti, A., Paladin, G., Vergassola, M., Vulpiani, A.: A random process for the construction of multiaffine fields. Physica D **65**, 352–358 (1993)
6. Benzi, R., Ciliberto, S., Tripicione, R., Baudet, C., Massaioli, F.: Extended self similarity in turbulent flows. Phys. Rev. E **48**, R29–R32 (1993)
7. Biermé, H., Meerschaert, M.M., Scheffler, H.P.: Operator scaling stable random fields. Stochastic Processes and their Applications **117**(3), 312–332 (2007)
8. Carey, W., Chuang, D., Hemami, S.: Regularity-preserving image interpolation. Image Processing, IEEE Transactions on **8**(9), 1293 –1297 (1999). DOI 10.1109/83.784441
9. Castaing, B., Dubrulle, B.: Fully developed turbulence : a unifying point of view. J. Phys. II France **5**, 895–899 (1995)
10. Castaing, B., Gagne, Y., Hopfinger, E.: Velocity probability density functions of high Reynolds number turbulence. Physica D **46**, 177–200 (1990)
11. Chainais, P.: Multidimensional infinitely divisible cascades. application to the modelling of intermittency in turbulence. Eur. J. Phys. B **51**, 229–243 (2006)
12. Chainais, P.: Infinitely divisible cascades to model the statistics of natural images. IEEE Trans. on Patt. and Mach. Intell. (2007). DOI 10.1109/TPAMI.2007.1113 (ISSN: 0162-8828)
13. Chainais, P., Riedi, R., Abry, P.: Scale invariant infinitely divisible cascades. In: Int. Symp. on Physics in Signal and Image Processing, Grenoble, France (2003)
14. Chainais, P., Riedi, R., Abry, P.: On non scale invariant infinitely divisible cascades. IEEE Transactions on Information Theory **51**(3), 1063–1083 (2005)
15. Chainais, P., Riedi, R., Abry, P.: Warped infinitely divisible cascades: beyond scale invariance. Traitement du Signal **22**(1) (2005)
16. Chang, S., Cvetkovic, Z., Vetterli, M.: Resolution enhancement of images using wavelet transform extrema extrapolation. In: Acoustics, Speech, and Signal Processing, 1995. ICASSP-95., 1995 International Conference on, vol. 4, pp. 2379 –2382 vol.4 (1995). DOI 10.1109/ICASSP.1995.479971
17. Decoster, N., Roux, S., Arneodo, A.: A wavelet-based method for multifractal image analysis. ii. applications to synthetic multifractal rough surfaces. Eur. Phys. J. B **15**, 739–764 (2000)
18. Delouille, V., Chainais, P., J.-F. Hochedez, J.F.: Quantifying and containing the curse of high resolution coronal imaging. Annales Geophysicae **26**(10), 3169–3184 (2008)
19. Ebert, D., Musgrave, F., Peachy, D., Perlin, K., Worley, S.: Texturing and Modeling: A Procedural Approach, third edn. Morgan Kaufmann (2003)
20. Fattal, R.: Image upsampling via imposed edge statistics. In: SIGGRAPH '07: ACM SIGGRAPH 2007 papers, p. 95. ACM, New York, NY, USA (2007). DOI http://doi.acm.org/10.1145/1275808.1276496
21. Feller, W.: An Introduction to Probability Theory and Its Applications, vol. 2. John Wiley and Sons, Inc., New-York, London, Sidney (1966)
22. Freeman, W.T., Jones, T.R., Pasztor, E.C.: Example-based superresolution. IEEE Computer Graphics and Applications **22**(2), 56–65 (2002)
23. Frisch, U.: Turbulence. The legacy of A. Kolmogorov. Cambridge University Press, Cambridge, UK (1995)

24. Glasner, D., Bagon, S., Irani, M.: Super-resolution from a single image. In: Computer Vision, 2009 IEEE 12th International Conference on, pp. 349 –356 (2009). DOI 10.1109/ICCV.2009.5459271
25. Grenander, U., Srivastava, A.: Probability models for clutter in natural images. IEEE Transactions on Pattern Analysis and Machine Intelligence **23**(4), 424–429 (2001)
26. Guofang, T., Zhang, C., Wu, J., Liu, X.: Remote sensing image processing using wavelet fractal interpolation. In: Proceedings of the International Conference on Communications, Circuits and Systems, vol. 2, p. 706 (2005). DOI 10.1109/ICCCAS.2005.1495209
27. HaCohen, Y., Fattal, R., Lischinski, D.: Image upsampling via texture hallucination. In: Proceedings of IEEE Int. Conf. on Computational Photography (2010)
28. Han, Z., Denney, T.J.: Incremental fourier interpolation of 2-d fractional brownian motion. Industrial Electronics, IEEE Transactions on **48**(5), 920 –925 (2001). DOI 10.1109/41.954556
29. Hochedez, J.F., et al.: Eui, the ultraviolet imaging telescopes of solar orbiter. In: Proceedings of the 2nd Solar Orbiter Workshop, vol. 641. ESA-SP, Athens (2006)
30. Jaffard, S.: Multifractal formalism for functions, part 1 & 2. SIAM J. of Math. Anal. **28**(4), 944–998 (1997)
31. Jaffard, S.: Beyond Besov spaces part 1: distributions of wavelet coefficients. The Journal of Fourier Analysis and Applications **10**(3), 221–246 (2004)
32. Jaffard, S.: Wavelet techniques in multifractal analysis. In: Fractal Geometry and Applications: A Jubilee of Benoît Mandelbrot, M. Lapidus & M. van Frankenhuijsen Eds., Proceedings of Symposia in Pure Mathematics, vol. 72(2), pp. 91–152. AMS (2004)
33. Kirshner, H., Porat, M.: On the role of exponential splines in image interpolation. Image Processing, IEEE Transactions on **18**(10), 2198 –2208 (2009). DOI 10.1109/TIP.2009.2025008
34. Kœnig, E., Chainais, P.: Virtual resolution enhancement of scale invariant textured images using stochastic processes. In: Proceedings of IEEE-ICIP 2009, Cairo (2009)
35. Kœnig, E., Chainais, P., Delouille, V., Hochedez, J.F.: Amélioration virtuelle de la résolution d'images du soleil par augmentation d'information invariante d'échelle. In: Proceedings of the 22nd Colloquium GRETSI, Dijon (2009)
36. Lashermes, B., Jaffard, S., Abry, P.: Wavelet leaders based multifractal analysis. In: Proc. of Int. Conf. on Acoustics, Speech and Signal Proc. Philadelphia, USA (2005)
37. Levy-Vehel, J., Legrand, P.: Hölderian regularity-based image interpolation. In: Proceedings of the IEEE International Conference on Acoustics, Speech and Signal Processing, ICASSP, vol. 3, pp. III –III (2006). DOI 10.1109/ICASSP.2006.1660788
38. Li, X.: Image resolution enhancement via data-driven parametric models in the wavelet space. EURASIP Journal on Image and Video Processing **2007**(41516), 12 p. (2007). DOI doi:10.1155/2007/41516
39. Li, X., Orchard, M.T.: New edge-directed interpolation. IEEE Transactions on Image Processing **10**, 1521–1527 (2001)
40. Liu, Y., Fieguth, P.: Image resolution enhancement with hierarchical hidden fields. In: ICIAR '09: Proceedings of the 6th International Conference on Image Analysis and Recognition, pp. 73–82. Springer-Verlag, Berlin, Heidelberg (2009). DOI http://dx.doi.org/10.1007/978-3-642-02611-9_8
41. Mandelbrot, B.: Intermittent turbulence in self-similar cascades: divergence of high moments and dimension of the carrier. J. of Fluid Mech. **62**, 331–358 (1974)
42. Muzy, J., Bacry, E.: Multifractal stationary random measures and multifractal random walks with log-infinitely divisible scaling laws. Phys. Rev. E **66**(056121) (2002)
43. Muzy, J., Bacry, E., Arneodo, A.: Multifractal formalism for fractal signals: The structure function approach versus the wavelet transform modulus-maxima method. J. Stat. Phys. **70**, 635–674 (1993)
44. Olshausen, B., Field, D.: Emergence of simple-cell receptive properties by learning a sparse code for natural images. Nature **381**, 607–609 (1996)
45. Portilla, J., Simoncelli, E.: A parametric texture model based on joint statistics of complex wavelet coefficients. Int. Journal of Computer Vision **40**(1), 49–71 (2000)
46. Riedi, R.H.: Multifractal processes. Long-range dependence : theory and applications (2001)
47. Schertzer, D., Lovejoy, S.: Physical modeling and analysis of rain and clouds by anisotropic scaling multiplicative processes. J. Geophys. Res. **92**, 9693 (1987)
48. Schmitt, F., Marsan, D.: Stochastic equations generating continuous multiplicative cascades. Eur. Phys. J. B **20**, 3–6 (2001)
49. Srivastava, A., Lee, A., Simoncelli, E., Zhu, S.C.: On advances in statistical modeling of natural images. Journal of mathematical imaging and vision **18**, 17–33 (2003)
50. Suetake, N., Sakano, M., Uchino, E.: Image super-resolution based on local self-similarity. Optical Review **15**, 26–30 (2008). DOI 10.1007/s10043-008-0005-0
51. Thevenaz, P., Blu, T., Unser, M.: Interpolation revisited [medical images application]. Medical Imaging, IEEE Transactions on **19**(7), 739–758 (2000). DOI 10.1109/42.875199
52. Turiel, A., Mato, G., Parga, N., Nadal, J.: Self-similarity properties of natural images resemble those of turbulent flows. Physical Review Letters **80**(5), 1098–1101 (1998)
53. Unser, M., Aldroubi, A., Eden, M.: Enlargement or reduction of digital images with minimum loss of information. IEEE Transactions on Image Processing **4**(3), 247–258 (1995)
54. Unser, M., Zerubia, J.: A generalized sampling theory without band-limiting constraints. IEEE Transactions on Circuits and Systems II **45**(8), 959–969 (1998)
55. Wainwright, M., Simoncelli, E.: Scale mixtures of gaussians and the statistics of natural images. Adv. Neural Information Processing Systems **12**, 855–861 (2000). NIPS'99
56. Wainwright, M., Simoncelli, E., Willsky, A.: Random cascades on wavelet trees and their use in analyzing and modeling natural images. Applied and Computational Harmonic Analysis **11**, 89–123 (2001)
57. Wendt, H., Roux, S.G., Abry, P., Jaffard, S.: Wavelet leaders and bootstrap for multifractal analysis of images. Signal Proces. **89**, 1100–1114 (2009)